Molecular Tethering Effect of C-Terminus of Amyloid Peptide Aβ42

Lei Liu,[†,‡,⊥] Lin Niu,[†,⊥] Meng Xu,[†] Qiusen Han,[†] Hongyang Duan,[†] Mingdong Dong,[§] Flemming Besenbacher,[§] Chen Wang,[*,†] and Yanlian Yang[*,†]

[†]National Center for Nanoscience and Technology, Beijing 100190, China, [‡]Institue for Advanced Materials, Jiangsu University, Zhenjiang 212013, China, and [§]Interdisciplinary Nanoscience Center (iNANO), Aarhus University, 8000 Aarhus C, Denmark. [⊥]These authors (L.L. and L.N.) contributed equally to this work.

ABSTRACT Amyloid peptides are considered to be the main contributor for the membrane disruption related to the pathogenesis of degenerative diseases. The variation of amino acids at the carboxylic terminus of amyloid peptide has revealed significant effects on the modulation of abnormal assemblies of amyloid peptides. In this work, molecular binding agents were tethered to the C-terminus of β-amyloid peptide 1−42 (Aβ42). The molecular interaction between Aβ42 and molecule tethers was identified at single molecule level by using scanning tunneling microscopy (STM). The mechanistic insight into the feature variation of the self-assembly of Aβ42 peptide caused by molecular tethering at C-terminus was clearly revealed, which could appreciably affect the nucleation of amyloid peptide, thus reducing the membrane disruptions.

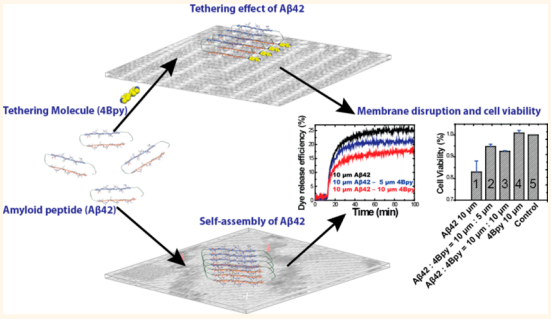

KEYWORDS: amyloid peptide · molecular tethering effect · peptide aggregation · modulation · membrane disruption

It has been documented that structural characteristic of protein can be tuned by variety of approaches such as protein modification[1] or molecular binding.[2] Previous studies have revealed that protein termini can be modified or bonded to regulate the biological activities of protein and peptides.[1,2] For instance, C-terminal α-amidation or phosphorylation[3] was shown to be essential for non-opioid peptide function or transcription transrepression, respectively. C-Terminal modification of antimicrobial cationic peptide can facilitate the improvement of outer membrane permeability.[4] Furthermore, the topology of membrane protein can be tuned by placing a single residue at C-terminus.[5] C-Terminus modifications could also provide a possible way to tune abnormal assemblies of protein such as amyloid peptides that are associated with the membrane disruption[6−8] and pathogenesis of degenerative diseases.[9]

β-Amyloid peptide 1−42 (Aβ42)[10,11] is one variant of the β-amyloid protein that was closely correlated to the pathogenesis of Alzheimer's Disease[12] (AD). On the basis of the amyloid cascade hypothesis,[13] the accumulation and deposition of misfolded Aβ42 in the brain have been proposed to be the key factor in the development of neurodegeneration. The dramatically reduced aggregation propensity and cytotoxicity of the shorter variants Aβ40 and Aβ39 with deletion of C-terminal residues compared to Aβ42[14,15] indicated that C-terminus may be a targeting site for tuning abnormal assemblies of amyloid peptides.

The self-assembled structures of Aβ42 such as soluble oligomers,[16] protofibrils,[17] and fibrils[18] have been reported to induce neurotoxicity at different levels. Modulating the assembly and aggregation of Aβ peptide by introducing bonded molecules will offer attractive opportunities for possible potential therapeutic intervention. Until now, a variety of molecules have been designed as molecular binding agents including organic molecule,[19−23] such as Congo red, thioflavin T (ThT), curcumin, and polyphenol. Many peptide motifs have also been explored targeting the core fragments of Aβ42, such as Aβ16−20[24] and Aβ14−23,[25] by X-ray diffraction[26,27] and theoretical simulations.[28] The critical effect of C-terminus of Aβ peptide on amyloid aggregation was addressed[14,15] previously. Therefore, it is plausible that aggregation kinetics and cellular effect of amyloid peptides are sensitively dependent on C-terminal segments. However, the utilization

* Address correspondence to wangch@nanoctr.cn, yangyl@nanoctr.cn.

Received for review July 9, 2014 and accepted September 5, 2014.

Published online September 05, 2014
10.1021/nn503737r

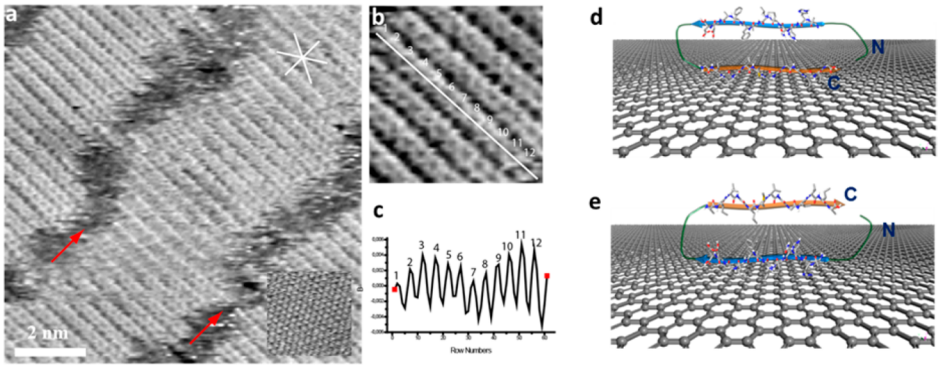

Figure 1. (a) STM image of two-dimensional assemblies of Aβ42 on HOPG surface. (b) High-resolution STM images of Aβ42. The tunneling conditions: I = 919.2 pA, V = −418.5 mV. (c) The Fourier transformation analysis of peptide strand observed in (b). Two possible basic building models for Aβ42 assemblies on HOPG surface: (d) segment 33−42 adsorbed on HOPG and (e) segment 1−20 adsorbed on HOPG. The full sequence of Aβ42 is imposed on the model.

of C-terminus modulation for tuning amyloid assembly and its underlying molecular mechanistic insight have not been fully explored yet.

Herein, we investigate the modulating effect on Aβ42 peptide assembly and the aggregation by a tethering molecule 4,4′-bipyridyl (4Bpy) to C-terminus of Aβ42. The hydrogen bonds between 4Bpy and Aβ42 at C-terminus were revealed at single molecular level by using scanning tunneling microscopy (STM). In this way, one could differentiate individual amino acid,[29] analyze the mechanism of peptide assembly[30−32] and understand the interaction between the peptides and molecules.[31] The tethering of 4Bpy to C-terminus of Aβ42 was shown to significantly affect the assembling characteristics of Aβ42, as well as the aggregation kinetics. As the result, the reduction of membrane disruption of Aβ42 in the presence of 4Bpy molecule can be identified, even in depressing the cytotoxicity of Aβ42.

RESULTS AND DISCUSSION

Individual Aβ42 molecules could be observed to assemble into lamellar structures with submolecular resolution (Figure 1a), when deposited on the surface of highly oriented pyrolytic graphite (HOPG). These assemblies are probably the β-sheet structures formed by Aβ42 hairpins,[33] as one arm of the hairpin is in contact with the graphite surface.[30] Striped structures comprising β-strands represented by bright features parallel to each other can be clearly observed, and the hairpin skeletons are nearly perpendicular to the stripe axis and cannot be resolved in the STM image. The β-turn and random-coil regions of the Aβ42 hairpins are located in the grooves, which is consistent with the previous reports.[30,34]

Separations between two parallel neighboring stripes are measured to be nearly the same at 0.47 ± 0.05 nm, which is identical to the previously reported spacing between two neighboring hydrogen-bonded β-strands consisting of the fibrils.[35] The measured length range of Aβ42 β-strands from experimental STM data are listed in Supporting Information Table S1 and Figure S1. The distribution shows the apparent length of Aβ42 peptide β-strand, which one is adsorbed on the HOPG surface, ranging from 2.2 to 4.5 nm. The separation between the two neighboring amino acids with peptide chain structures is 0.325 nm for the parallel β-sheet structures.[36] The number of amino acids in the core regions of the Aβ_{42} hairpins was calculated to be narrowly distributed around the mean value of 9−15 residues. The difference in the length of β-strands was also reflected in the ragged lamellar structures observed in Figure 1a, which can be mainly due to the folding multiplicity[30] by the competition of peptide intramolecular force, subsequently be assembled into two-dimensional lamellae on the surface.

From the high-resolution view of Aβ42 lamella (Figure 1b), we can observe that every β-strand are represented as bright double-dotted ribbons and one pair of bright spots represent one amino acid residue. The periodicity of single β-strand of peptide was revealed by Fourier transform analysis (Figure 1c), and each peak represents one residue of peptide, which is also consistent with the observation from STM image. According to the above discussion, the schematic model of Aβ42 assembly on the HOPG surface is proposed in Figure 1d,e. Because Aβ42 is a β-hairpin structure, there are two adsorption configuration possibilities: N-terminal contacting (Figure 1d) and C-terminal contacting (Figure 1e).

To tune the assemblies of Aβ42 at molecular level, molecular tether 4Bpy was introduced. The continuous and highly periodic arrangements of Aβ42/4Bpy coassembly on HOPG surface was observed by STM (Figure 2a). It was deduced that the characteristic of Aβ42 molecules can be modulated by a novel arrangement when mixed with specific binding agent. The features with higher contrast in the linear array are attributed to 4Bpy molecules and the stripes with lower contrast are associated with Aβ42. As a conjugated π-electron system, 4Bpy tends to give higher electron conductance,

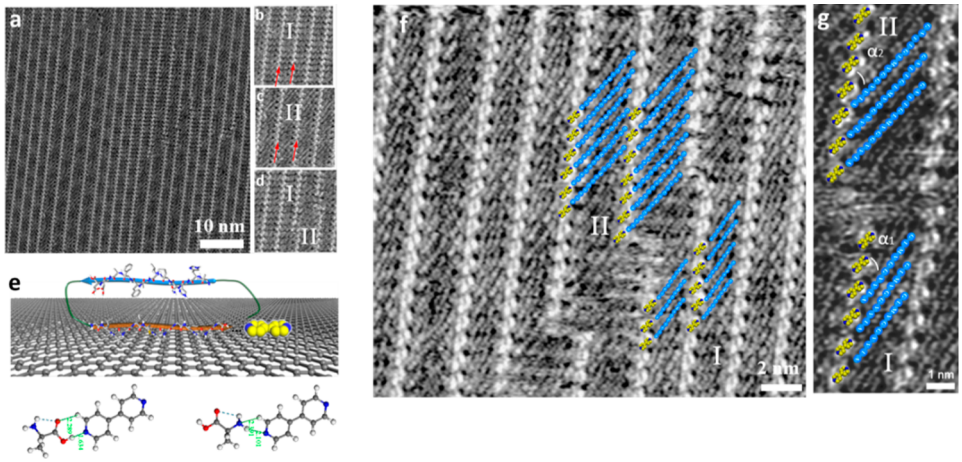

Figure 2. (a) A large-scale STM image containing all kinds of Aβ42/4Bpy coassemblies and high-resolution STM images of Aβ42/4Bpy coassemblies: (b) type I lamella, (c) type II lamelle, and (d) type I and type II lamella. (e) The basic building model for Aβ42/4Bpy coassemblies on HOPG surface. The theoretical calculation of binding energy of amino acid two termini with nitrogen atom of 4,4′-bipyridyl molecule. (Left bottom of e) C-terminus of amino acid with nitrogen atom of 4Bpy molecule, E = 0.78 eV. (Right bottom of e) N-terminus of amino acid with nitrogen atom of 4Bpy molecule, E = 0.42 eV. The distance of intermolecular hydrogen bond is displayed in green dashed line. (f and g) The high-resolution STM image of Aβ42/4Bpy coassemblies with basic building models. The molecular structures of Aβ42 and 4,4′-bipyridyl are provided in (e−g). The hairpin structure with blue and gray circles is for the full sequence of Aβ_{42} imposed on the model and the yellow circles for the pyridyl rings in (e). The blue stripes stand for the β-strands with amino acid sequence adsorbed on the HOPG surface and the yellow circles for the pyridyl rings. The 4Bpy molecules bind to the amyloidogenic peptide Aβ42 *via* carboxyl groups of Aβ42. The details for type I and type II lamellae: the length of the beta strands adsorbed on the HOPG surface is 2.76 ± 0.17 nm (10 residues) for type I and 4.06 ± 0.17 nm (14 residues) for type II; the angles of the peptide molecule to the 4Bpy axis are approximately 25° in type I and 33° in type II. The tunneling conditions: I = 299.1 pA, V = 799.9 mV.

and thus, it appears brighter in STM images (Figure 2a−d). This coassembled lamella structure can be ascribed to the hydrogen bonds between the termini of Aβ42 and the nitrogen atom of 4Bpy molecule. The interaction between amino acid termini and 4Bpy molecules is theoretically calculated by density functional theory (DFT) method. The binding energy between the C-terminus and 4Bpy is 0.78 eV, which is much higher than the one (0.48 eV) between the N-terminus and 4Bpy (Figure 2e). It implied that 4Bpy molecule would prefer to bind to C-terminus rather than N-terminus of peptide, which is also consistent with previous reports.[31,32] The tethering of two neighboring C-termini of Aβ42 helps to stabilize the C-terminal β-stand of Aβ42. It is therefore also deduced that C-terminal β-stands contact the surface while Aβ42 self-assemble and coassemble with molecules as proposed in structural model superimposed in Figure 2e.

Significant differences between the lamellae assembled from Aβ42/4Bpy and the one composed of Aβ42 (Figure 2b−d) should be noticed. On the basis of the high-resolution view of Aβ42/4Bpy coassembled lamella (Figure 2f), two characteristic types of assembled structures were presented in case of molecular binding of 4Bpy to C-terminus of Aβ42 (Figure 2b−d,f). Compared to Aβ42 assembled lamella, Aβ42/4Bpy coassemblies present more ordered structures by molecular tethering. After the statistical analysis, the apparent length of Aβ42 β-strand that adsorbed on the HOPG surface in the coassembly ranges from 2.9 to 4.2 nm and the β-strands of the Aβ42 hairpins in the Aβ42/4Bpy coassembly were mainly composed of 10, 11, and 14 residues (Supporting Information Table S2 and Figure S2). The amino acids number of the β-strands of the Aβ42 hairpins was mainly 10/11 residues (accounting for 44.1% in the β-strands observed by STM) in type I coassembly, and 14 residues (accounting for 54.1% in the β-strands observed by STM) in type II coassembly. In the presence of the tethering molecule, the assembling characteristic of peptides was changed due to the molecular tethering effect. The delicate balance of molecular interactions between the peptide backbones such as hydrophobic interaction, salt-bridge, and intermolecular hydrogen bond might enable peptide to self-assemble in a different way. The peptide strand with lengths other than 10/11 and 14 may be energetically unstable, and not involved in the coassemblies after molecular tethering. The other difference between type I and II structures lies in the angle between the bonded Aβ42 molecules and the molecular axis of the stripe. In type I structure, the angle of the peptide molecule to the axis is approximately 25°, whereas the value is 33° in type II one. Both angles are totally distinct from the one (∼90°) between Aβ42 molecule and stripe axis in pure peptide assemblies (Figure 1a). Molecule tethers binding to the C-terminus of Aβ42 enabled the peptides to self-assemble in different ways compared to the Aβ42 assembly alone, which was summarized in Table 1.

TABLE 1. Summary of Difference of Molecular Self-Assembly between Aβ42 and Aβ42 Tuned by 4Bpy

Molecules \ Assembly feature	Core region length (residue number)	Angle of peptide to stripe axis	Building units for the assembly
Aβ42	10-15	90° ± 4 °	
Aβ42 / 4Bpy	Type I: (10 and 11)	Type I: (25° ± 1°)	
	Type II: (14)	Type II: (33° ± 2°)	

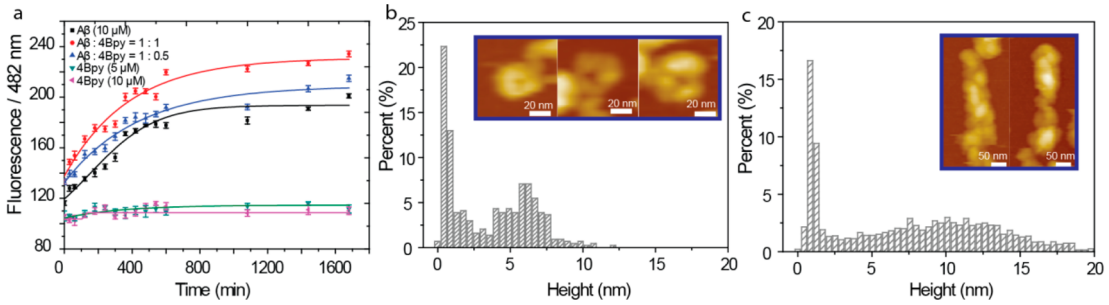

Figure 3. Aggregation behaviors and self-assembled nanostructures of Aβ42 in bulk solution before and after molecular binding. (a) The ThT assay of the self-assembly process of Aβ42 (10 μM), Aβ42 with 4Bpy molecule (10 μM:10 μM), Aβ42 with 4Bpy molecule (10 μM:5 μM), 4Bpy molecule (5 μM), 4Bpy molecule (10 μM). Molecular tuning could obviously increase the aggregation of Aβ42. Topography images and height distributions of (b) Aβ42 oligomers incubated for 2 h in PBS solution, (c) Aβ42 aggregates incubated for 2 h tuned by 4Bpy molecule in PBS solution. All the AFM images of Aβ42 assemblies on mica surface were obtained in liquid.

All these differences occurring in Aβ42 assemblies are mainly due to the C-terminal molecular binding effect on Aβ42 assembly. C-terminus of amyloid peptide is critical for the assembly formation.[14] This result is in agreement with previously reported folding site variations between Aβ40 and Aβ42 with two residues difference, isoleucine and alanine, which consists of β-strands with residues 12−24/30−40[35] in Aβ40 and residues 18−26/31−42[33] in Aβ42. It was anticipated that the intermolecular interaction between the strands of Aβ in the assemblies was modulated, which resulted in the different aggregation between Aβ40 and Aβ42. It is of significance that the interaction between the amyloid peptide was affected after the molecular binding.

The angle of the peptide to the axis of assembling stripe and core length of β-strands were both tuned, which results from the interaction between the peptides and 4Bpy at the Aβ42 C-terminus. The tethering molecule binding to the C terminus of peptide by the intermolecular hydrogen bond enables the rearrangement of the peptide assemblies, such as the amino acid mismatch between the peptide backbones (Figure 2f,g and Figure 1a) and the adjustment of hydrophobic interactions between the β-strands to some extent. These variations in geometrical arrangement and the orientation to the surface leads to the distinct building units for modulated peptide assembly. The high-resolution structural images obtained by STM provide useful insight that the new constructed building units *via* interaction between Aβ42 and 4Bpy molecule by C-terminal binding are very likely to influence the aggregation of amyloid peptides in aqueous solution.

To assess the impact of C-terminal molecular binding approach, ThT assay was performed to visualize and quantify the aggregation of amyloid protein with and without 4Bpy molecules. Aβ42 (10 μM) aggregated quickly (Figure 3a), which is consistent with the previous report[37] and the amyloid fibrils were obtained (Supporting Information Figure S3). However, it can be clearly observed that the introduction of molecular tether 4Bpy could appreciably promote the aggregation of Aβ42 in solution mainly due to the molecular binding between Aβ42 and 4Bpy molecule (Figure 3a). The stoichiometry of Aβ42 and 4Bpy molecule (1:1) clearly showed much better impact on promoting the aggregation of Aβ42 compared to the molar ratio 2:1. It is suggested that the optimized molecular binding ratio of 4Bpy to Aβ42 could be 1:1. The plateau of aggregation of Aβ42 was increased in the presence of 4Bpy, compared to bare Aβ42 peptide aggregation. To form protein aggregates with distinct morphology is implied. The assembled nanostructure of Aβ42 was indeed tuned by molecular binding at C-terminus, which was observed by atomic force microscopy (AFM) in liquid to avoid the surface and volatilization effect (Figure 3b,c). Annular-like oligomers was obtained and presented after incubating Aβ42 for 2 h, and the height was determined to be ~6 nm and the diameter was ~50 nm (Figure 3b).

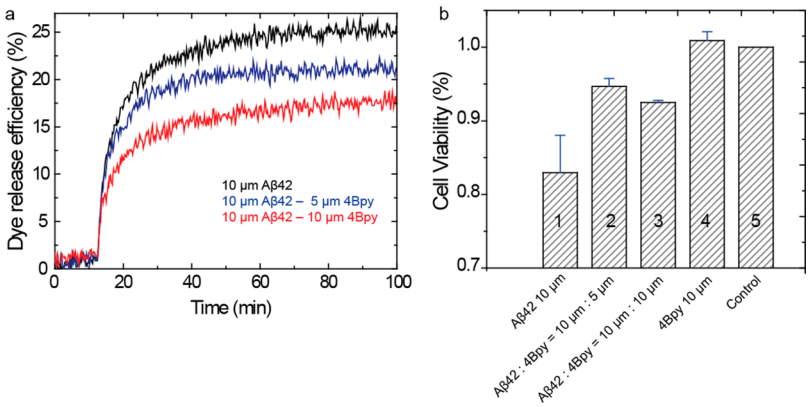

Figure 4. Assay of the disruption of liposome membrane and the cytotoxicity of SH-SY5Y cells induced by Aβ42 and Aβ42/4Bpy solutions. (a) The calcein dye release efficiency of liposome trigged by Aβ42 (black line) and Aβ42 tuned by 4Bpy molecules (blue line and red line). The concentrations for the comparison of the dye release efficiency of Aβ42 and Aβ42/4Bpy are 10 μM (black), 10 μM:5 μM (blue), and 10 μM:10 μM (red). All the samples have been shaken and incubated for 2 h at 37 °C. (b) The cytotoxicity of (1) Aβ42 oligomers, (2−3) Aβ42 modified with 4Bpy molecules, and (4) 4Bpy molecules measured by WST-8 toxicity assay. The concentrations for the comparison of the cytotoxicity of Aβ42, Aβ42/4Bpy, and 4Bpy are 10 μM (1), 10 μM:5 μM (2) and 10 μM:10 μM (3), and 10 μM (4), respectively. Results are means ± SD (n = 3). (5) The blank control.

C-Terminal binding agent did facilitate the modulation of the assembly of Aβ42 which is revealed by the promoted aggregation from initial stage (Figure 3a). The tuned assembled amyloid oligomers of Aβ42 with the height of ~12 nm and the width of about 100 nm were obviously observed and they were considered to be the aggregates with higher degree of polymerization. It is therefore plausible to imply that molecular tethering at C-terminus of Aβ42 could be employed to efficiently modulate the aggregation of amyloid peptide.

To verify the variations of the activity of Aβ42 on the membrane surface after molecular binding at C-terminus, the membrane permeability,[38,39] as well as the cell viability, was examined in the presence of Aβ42 oligomer and the molecularly tethered Aβ42 aggregates. We initially monitored the release of fluorescence probe calcein entrapped in liposomes triggered by Aβ42 oligomers and Aβ42/4Bpy aggregates. We did observe appreciably higher permeability resulting from the Aβ42 oligomers incubated for 2 h at the concentration of 10 μM (black line in Figure 4a), rather than the Aβ42 fibrils (Supporting Information Figure S4). The membrane disruption of Aβ42 aggregates was slightly relieved in case of 5 μM 4Bpy introduction. Even more pronounced decrease of fluorescence signal was observed with the concentration of 4Bpy up to 10 μM (red line in Figure 4a), which indicated the reduction of the membrane permeability. The decreased membrane permeability by molecular modulation implies a reduced cytotoxicity. To validate the cell biological effect of the molecular tethering, the cytotoxicity of Aβ42 and Aβ42/4Bpy aggregates was assessed by cell viability assay. The cell viability of SH-SY5Y neuroblastoma cells treated with Aβ42 oligomers (10 μM) was lower and a significant difference was observed compared to the control species. Treatment of the cells with Aβ42/4Bpy (10 μM:5 μM) and Aβ42/4Bpy (10 μM:10 μM) resulted in the relatively high cell viabilities, which presented the lower cytotoxicity than Aβ42 oligomers (Figure 4b). Combined with the membrane permeability assay, it is deduced that the tuned Aβ42 assemblies (Aβ42/4Bpy) with larger size revealed in AFM results (Figure 3c) possess the weak ability of membrane disruption, resulting in the lower cytotoxicity. The introduction of 4Bpy molecule binding to Aβ42 at C-terminus can enhance the multiple interactions between the peptide assemblies, further facilitating the accelerated aggregation of Aβ42, which results in larger aggregates rather than the toxic oligomers. It is therefore plausible to explain how the molecule binds at C-terminus of the peptide in Aβ42 assemblies and neutralizes the cytotoxicity of amyloid aggregates.

CONCLUSION

To sum up, tuning the Aβ42 self-assemblies by molecular tethering at the C-terminus of peptide was achieved and visualized by STM at the molecular level in this work, which provided insights into the molecular mechanism responsible for the modulation of amyloid peptide assemblies. The annular oligomer with small size of Aβ42 was appreciably varied to the particles with wider size distribution with the molecular tethering, which did further promote the Aβ42 aggregation. Finally, the reduced membrane disruption and cytotoxicity of Aβ42 was achieved by the molecular binding at C-terminus, which is associated with the accelerated aggregation process of amyloid peptide. The approach we proposed evidently addressed the fact that small molecules introduced to bind with the termini of amyloid protein would offer a promising opportunity for therapeutic intervention of AD and other degenerative diseases. This simple but intriguing strategy

provides a wealth of possibilities in molecular design for amyloid proteins targeting, aggregation modulation and some potential therapeutic applications. Furthermore, these findings also paved the way for molecular design in tuning peptide self-assemblies for constructing multifunctional nanomaterials.

EXPERIMENTAL SECTION

Peptide Sample Preparation for STM Investigation. Aβ42 was purchased from American Peptide Company, Inc. with a purity of 98%. Hexafluoroisopropyl alcohol (HFIP, Sigma) as the solvent was used to dissolve Aβ42 initially for an extended time, and the solution was transferred into a sterile microcentrifuge tube followed by evaporation of HFIP solvent under vacuum. The obtained peptide deposits were dissolved in Milli-Q water. 4Bpy (Sigma) was first dissolved in ethanol, and then the peptide solutions or peptide/pyridyl molecule mixed solutions reach the final concentration of *ca.* 10 μM. The sample solutions were kept at 37 °C for 2 h; then, 5 μL of Aβ42 solutions or peptide/molecule complex solutions was dropped onto a freshly cleaved HOPG surface it and observed directly by STM after the solvent was fully evaporated.

STM Experiments. The STM experiments were carried out with a Nanoscope IIIa system (Bruker Nano Surfaces) working at ambient conditions. Mechanically formed Pt/Ir (80%/20%) tips were used in the STM experiments. All STM images were obtained in constant current mode, and the tunneling conditions were shown in the corresponding figure captions.

AFM Investigation in Liquid. Aβ42 solution with concentration of 10 μM in phosphate buffer saline (PBS buffer, pH 7.4) and the mixture of Aβ42/4Bpy (10 μM:10 μM) were incubated for 2 h and ready for AFM investigations. Five microliters of each sample droplet was dropped onto newly cleaved mica substrate. Ten minutes later, 50 μL of imaging buffer PBS was added to the substrate before AFM measurement. All AFM images were recorded under liquid conditions. In liquid imaging, ultrasharp silicon cantilevers (triangular, OMCL-TR400PSA-1, Olympus) were used with a typical resonance frequency of 34 kHz, a spring constant of 0.08 N/m, and a nominal tip radius of 15 nm. All the AFM images were acquired in the tapping mode at a scan frequency of 1 Hz with an applied minimal loading force of 100 pN and optimized feedback parameters in buffer. The resolution of all the AFM images was 512 $\times$ 512 pixels per image. The images were flattened and analyzed automatically by using the commercial software Scanning Probe Image Processor (SPIPTM, Image Metrology ApS, version5.1.3, Lyngby, Denmark).

Density Functional Theory (DFT) Calculation. The first-principles DFT calculations for 4Bpy and amino acid were performed with the *DMol* module in Materials Studio. The generalized gradient approximation with the PW91 functional was used to describe the exchange-correlation effects. In this study a double numerical basis set with polarization functions (DNP) was used. The sizes of the DNP basis sets are comparable with the 6-31G** basis and believed to be much more accurate than Gaussian basis sets of the same size. The tolerances of energy, gradient, and displacement convergence were 1×10^{-5} hartree, 2×10^{-3} hartree/Å, and 5×10^{-3} Å, respectively.

ThT Fluorescence Assay. Aβ42 was dissolved in HFIP to the concentration of 1 mg/mL and it was stored at 4 °C. Before experiment, 75 μL of sample solution was taken out from stock solution and dried by N_2 flow carefully. Subsequently, 7.5 μL of dimethyl sulfoxide (DMSO) was added to dissolve peptides, which were then diluted 1:200 into 50 mM PBS buffer (pH 7.4) or the one including 4Bpy with concentration of 10 μM and 5 μM, respectively. Finally, all the samples for ThT fluorescence assay were obtained such as Aβ42 solution with the concentration of 10 μM and the mixed solution of Aβ42/4Bpy (10 μM:10 μM and 10 μM:5 μM), 4Bpy solutions (5 μM and 10 μM). ThT fluorescence assay was performed in black fluorescence 96-well plate. Each sample was tested in 4 wells as repeated trial. A total of 180 μL of ThT (Sigma) and 20 μL of peptide solutions were added to each pore (the concentration of ThT solution was 10 μM). The fluorescence assay was tested by Tecan infinite M200 microplate reader. ThT fluorescence (excitation at 450 nm, emission at 482 nm) was measured at certain time intervals: 0, 0.5, 1, 2, 3, 4, 5, 6, 7, 8, 9, 10, 18, 24, and 28 h. The solution was incubated in shaker at 37 °C and 150 rpm. For the fluorescence, intensity was the average value of every sample at each time point.

Calcein Release Assay. 1,2-Dioleoyl-*sn*-glycero-3-phosphocoline (DOPC) and 1,2-dioleoyl-*sn*-glycero-3-[phospho-rac-(1-glycerol)] (DOPG) were obtained from Avanti Polar Lipids (Alabaster, AL). Five milligrams of dry lipid (DOPC:DOPG = 4:1) was transferred to a round-bottom glass flask and dissolved in an organic solvent containing methanol and chloroform (v/v = 1:1). Solvent was evaporated under a nitrogen flow while heated (37 °C). A thin film of lipid should appear when all solvent was evaporated. The flask was transferred to a vacuum-desiccator in order to get rid of the last traces of the organic solvent. Lipids were then resuspended by vortexing in 500 μL of Tris-HCl (20 mM, pH 7.5) containing 40 mM calcein sodium salt. The solution was exposed to at least seven cycles of freezing in liquid nitrogen, followed by thawing in a 50 °C water bath. Finally, the unilamellar vesicles including calcein were obtained.

Calcein-containing vesicles were added in the solution of Aβ42 and Aβ42/4Bpy by 5 s mixing and the release of calcein was measured using Tecan infinite M200 microplate reader at room temperature with excitation at 490 nm and emission at 520 nm. Data were collected every 11 s for 100 min until it reached a plateau.

Cell Viability Assay. SH-SY5Y cells were plated at a concentration of 10 000 cells/well (100 μL/well) in 96-well plates (Greiner Bio-, Inc., Longwood, FL) in full medium and the plates were incubated overnight at 37 °C. Then, SH-SY5Y neurons were treated with Aβ42 peptide (10 μM) with a 2 h incubation, Aβ42 in the presence of 4Bpy molecules (10 μM:5 μM and 10 μM:5 μM) with a 2 h incubation, and pure 4Bpy solution (10 μM). The WST-8 cell viability assay was performed by using Cell Counting Kit-8 (Dojindo Laboratories, Kumanoto, Japan), according to the supplier recommendations. Cell viability was expressed as the percentage of viable cell relative to untreated cells using the absorbance at 450 nm. Statistical analysis: experiments are means of triplicates. Data are expressed as mean $\pm$ standard deviation (SD). Statistical analyses were performed with SPSS (SPSS, Chicago) by using a paired *t* test. Differences were considered statistically significant when $P < 0.05$.

Conflict of Interest: The authors declare no competing financial interest.

Acknowledgment. This work was supported by National Natural Science Foundation of China (Grant Nos. 91127043, 21261130090). The National Basic Research Program of China (2011CB932800) is also gratefully acknowledged. L.L. acknowledges Jiangsu University Start Foundation for Talented Researcher (14JDG021).

Supporting Information Available: The distribution of the apparent core regions of Aβ42 chains, the main distribution of the fragments containing C-termini of Aβ42 chains with 4Bpy molecules, the amyloid fibrils observed by AFM, and the dye release efficiency of liposome trigged Aβ42 fibril solution. This material is available free of charge *via* the Internet at http://pubs.acs.org.

REFERENCES AND NOTES

1. Seizinger, B. R.; Liebisch, D. C.; Gramsch, C.; Herz, A.; Weber, E.; Evans, C. J.; Esch, F. S.; Bohlen, P. Isolation and Structure of a Novel C-Terminally Amidated Opioid Peptide, Amidorphin, from Bovine Adrenal Medulla. *Nature* **1985**, *313*, 57–59.

2. Abraha, A.; Kuret, J.; Binder, L. I. C-Terminus Truncation and Phosphorylation of the Human Tau Protein Enhances Tau Polymerization: An *In Vitro* Study Using Laser Light Scattering and Electron Microscopy. *J. Neurochem.* **2000**, *74*, S15–S15.
3. Rivka. Ofir; Dwarki, V. J.; Rashid, D.; Verma, I. M. Phosphorylation of the C Terminus of Fos Protein Is Required for Transcriptional Transrepression of the C-Fos Promoter. *Nature* **1990**, *348*, 80–82.
4. Piers, K. L.; Brown, M. H.; Hancock, R. E. Improvement of Outer Membrane-Permeabilizing and Lipopolysaccharide-Binding Activities of an Antimicrobial Cationic Peptide by C-Terminal Modification. *Antimicrob. Agents Chemother.* **1994**, *38*, 2311–2316.
5. Seppala, S.; Slusky, J. S.; Lloris-Garcera, P.; Rapp, M.; von Heijne, G. Control of Membrane Protein Topology by a Single C-Terminal Residue. *Science* **2010**, *328*, 1698–1700.
6. Lashuel, H. A.; Hartley, D.; Petre, B. M.; Walz, T.; Lansbury, P. T. Neurodegenerative Disease—Amyloid Pores from Pathogenic Mutations. *Nature* **2002**, *418*, 291–291.
7. Quist, A.; Doudevski, L.; Lin, H.; Azimova, R.; Ng, D.; Frangione, B.; Kagan, B.; Ghiso, J.; Lal, R. Amyloid Ion Channels: A Common Structural Link for Protein-Misfolding Disease. *Proc. Natl. Acad. Sci. U.S.A.* **2005**, *102*, 10427–10432.
8. Butterfield, S. M.; Lashuel, H. A. Amyloidogenic Protein Membrane Interactions: Mechanistic Insight from Model Systems. *Angew. Chem., Int. Ed.* **2010**, *49*, 5628–5654.
9. Laganowsky, A.; Liu, C.; Sawaya, M. R.; Whitelegge, J. P.; Park, J.; Zhao, M. L.; Pensalfini, A.; Soriaga, A. B.; Landau, M.; Teng, P. K.; *et al.* Atomic View of a Toxic Amyloid Small Oligomer. *Science* **2012**, *335*, 1228–1231.
10. Roberson, E. D.; Mucke, L. 100 Years and Counting: Prospects for Defeating Alzheimer's Disease. *Science* **2006**, *314*, 781–784.
11. Goedert, M.; Spillantini, M. G. A Century of Alzheimer's Disease. *Science* **2006**, *314*, 777–781.
12. Brody, D. L.; Magnoni, S.; Schwetye, K. E.; Spinner, M. L.; Esparza, T. J.; Stocchetti, N.; Zipfel, G. J.; Holtzman, D. M. Amyloid-Beta Dynamics Correlate with Neurological Status in the Injured Human Brain. *Science* **2008**, *321*, 1221–1224.
13. Hardy, J.; Selkoe, D. J. Medicine - the Amyloid Hypothesis of Alzheimer's Disease: Progress and Problems on the Road to Therapeutics. *Science* **2002**, *297*, 353–356.
14. Joseph, T.; Jarrett, E. P.; Berger, P. T.; Lansbury, J. The Carboxy Terminus of the Amyloid Protein Is Critical for the Seeding of Amyloid Formation: Implications for the Pathogenesis of Alzheimer's Disease. *Biochemistry* **1993**, *32*, 4693–4697.
15. Lansbury, P. T., Jr.; Costa, P. R.; Griffiths, J. M.; Simon, E. J.; Auger, M.; Halverson, K. J.; Kocisko, D. A.; Hendsch, Z. S.; Ashburn, T. T.; Spencer, R. G.; *et al.* Structural Model for the Beta-Amyloid Fibril Based on Interstrand Alignment of an Antiparallel-Sheet Comprising a C-Terminal Peptide. *Nat. Struct. Mol. Biol.* **1995**, *2*, 990–998.
16. Lambert, M. P.; Barlow, A. K.; Chromy, B. A.; Edwards, C.; Freed, R.; Liosatos, M.; Morgan, T. E.; Rozovsky, I.; Trommer, B.; Viola, K. L.; *et al.* Diffusible, Nonfibrillar Ligands Derived from a Beta(1−42) Are Potent Central Nervous System Neurotoxins. *Proc. Natl. Acad. Sci. U.S.A.* **1998**, *95*, 6448–6453.
17. Stroud, J. C.; Liu, C.; Teng, P. K.; Eisenberg, D. Toxic Fibrillar Oligomers of Amyloid-Beta Have Cross-Beta Structure. *Proc. Natl. Acad. Sci. U.S.A.* **2012**, *109*, 7717–7722.
18. Irie, K.; Murakami, K.; Masuda, Y.; Morimoto, A.; Ohigashi, H.; Ohashi, R.; Takegoshi, K.; Nagao, M.; Shimizu, T.; Shirasawa, T. Structure of Beta-Amyloid Fibrils and Its Relevance to Their Neurotoxicity: Implications for the Pathogenesis of Alzheimer's Disease. *J. Biosci. Bioeng.* **2005**, *99*, 437–447.
19. Frid, P.; Anisimov, S. V.; Popovic, N. Congo Red and Protein Aggregation in Neurodegenerative Diseases. *Brain Res. Rev.* **2007**, *53*, 135–160.
20. Klunk, W. E.; Debnath, M. L.; Pettegrew, J. W. Development of Small-Molecule Probes for the Beta-Amyloid Protein of Alzheimers Disease. *Neurobio. Aging.* **1994**, *15*, 691–698.
21. Yang, F. S.; Lim, G. P.; Begum, A. N.; Ubeda, O. J.; Simmons, M. R.; Ambegaokar, S. S.; Chen, P. P.; Kayed, R.; Glabe, C. G.; Frautschy, S. A.; *et al.* Curcumin Inhibits Formation of Amyloid Beta Oligomers and Fibrils, Binds Plaques, and Reduces Amyloid *in Vivo*. *J. Biol. Chem.* **2005**, *280*, 5892–5901.
22. Hamaguchi, T.; Ono, K.; Murase, A.; Yamada, M. Phenolic Compounds Prevent Alzheimer's Pathology through Different Effects on the Amyloid-Beta Aggregation Pathway. *Am. J. Pathol.* **2009**, *175*, 2557–2565.
23. Gestwicki, J. E.; Crabtree, G. R.; Graef, I. A. Harnessing Chaperones to Generate Small-Molecule Inhibitors of Amyloid Beta Aggregation. *Science* **2004**, *306*, 865–869.
24. Wu, W. H.; Lei, P.; Liu, Q.; Hu, J.; Gunn, A. P.; Chen, M. S.; Rui, Y. F.; Su, X. Y.; Xie, Z. P.; Zhao, Y. F.; *et al.* Sequestration of Copper from Beta-Amyloid Promotes Selective Lysis by Cyclen-Hybrid Cleavage Agents. *J. Biol. Chem.* **2008**, *283*, 31657–31664.
25. Takahashi, T.; Ohta, K.; Mihara, H. Embedding the Amyloid Beta-Peptide Sequence in Green Fluorescent Protein Inhibits Abeta Oligomerization. *ChemBioChem* **2007**, *8*, 985–988.
26. Biancalana, M.; Makabe, K.; Koide, A.; Koide, S. Molecular Mechanism of Thioflavin-T Binding to the Surface of Beta-Rich Peptide Self-Assemblies. *J. Mol. Biol.* **2009**, *385*, 1052–1063.
27. Biancalana, M.; Koide, S. Molecular Mechanism of Thioflavin-T Binding to Amyloid Fibrils. *Biochim. Biophys. Acta, Proteins Proteomics* **2010**, *1804*, 1405–1412.
28. Childers, W. S.; Mehta, A. K.; Lu, K.; Lynn, D. G. Templating Molecular Arrays in Amyloid's Cross-Beta Grooves. *J. Am. Chem. Soc.* **2009**, *131*, 10165–10172.
29. Claridge, S. A.; Thomas, J. C.; Silverman, M. A.; Schwartz, J. J.; Yang, Y. L.; Wang, C.; Weiss, P. S. Differentiating Amino Acid Residues and Side Chain Orientations in Peptides Using Scanning Tunneling Microscopy. *J. Am. Chem. Soc.* **2013**, *135*, 18528–18535.
30. Ma, X. J.; Liu, L.; Mao, X. B.; Niu, L.; Deng, K.; Wu, W. H.; Li, Y. M.; Yang, Y. L.; Wang, C. Amyloid Beta (1−42) Folding Multiplicity and Single-Molecule Binding Behavior Studied with STM. *J. Mol. Biol.* **2009**, *388*, 894–901.
31. Liu, L.; Zhang, L.; Niu, L.; Xu, M.; Mao, X. B.; Yang, Y. L.; Wang, C. Observation of Reduced Cytotoxicity of Aggregated Amyloidogenic Peptides with Chaperone-Like Molecules. *ACS Nano* **2011**, *5*, 6001–6007.
32. Liu, L.; Zhang, L.; Mao, X. B.; Niu, L.; Yang, Y. L.; Wang, C. Chaperon-Mediated Single Molecular Approach toward Modulating a Beta Peptide Aggregation. *Nano Lett.* **2009**, *9*, 4066–4072.
33. Luhrs, T.; Ritter, C.; Adrian, M.; Riek-Loher, D.; Bohrmann, B.; Doeli, H.; Schubert, D.; Riek, R. 3D Structure of Alzheimer's Amyloid-Beta(1−42) Fibrils. *Proc. Natl. Acad. Sci. U.S.A.* **2005**, *102*, 17342–17347.
34. Mao, X. B.; Wang, C. X.; Wu, X. K.; Ma, X. J.; Liu, L.; Zhang, L.; Niu, L.; Guo, Y. Y.; Li, D. H.; Yang, Y. L.; *et al.* Beta Structure Motifs of Islet Amyloid Polypeptides Identified through Surface-Mediated Assemblies. *Proc. Natl. Acad. Sci. U.S.A.* **2011**, *108*, 19605–19610.
35. Petkova, A. T.; Ishii, Y.; Balbach, J. J.; Antzutkin, O. N.; Leapman, R. D.; Delaglio, F.; Tycko, R. A Stru ctural Model for Alzheimer's Beta-Amyloid Fibrils Based on Experimental Constraints from Solid State NMR. *Proc. Natl. Acad. Sci. U.S.A.* **2002**, *99*, 16742–16747.
36. Pauling, L.; Corey, R. B. Two Rippled-Sheet Configurations of Polypeptide Chains, and a Note about the Pleated Sheets. *Proc. Natl. Acad. Sci. U.S.A.* **1953**, *39*, 253–256.
37. Liu, R.; Barkhordarian, H.; Emadi, S.; Park, C. B.; Sierks, M. R. Trehalose Differentially Inhibits Aggregation and Neurotoxicity of Beta-Amyloid 40 and 42. *Neurobiol. Dis.* **2005**, *20*, 74–81.
38. Vad, B.; Thomsen, L. A.; Bertelsen, K.; Franzmann, M.; Pedersen, J. M.; Nielsen, S. B.; Vosegaard, T.; Valnickova, Z.;

Skrydstrup, T.; Enghild, J. J.; *et al.* Divorcing Folding from Function: How Acylation Affects the Membrane-Perturbing Properties of an Antimicrobial Peptide. *Biochim. Biophys. Acta, Proteins Proteomics* **2010**, *1804*, 806–820.
39. Vad, B. S.; Bertelsen, K.; Johansen, C. H.; Pedersen, J. M.; Skrydstrup, T.; Nielsen, N. C.; Otzen, D. E. Pardaxin Permeabilizes Vesicles More Efficiently by Pore Formation than by Disruption. *Biophys. J.* **2010**, *98*, 576–585.